The RSLQR Control Method Based on the Linear Extended State Observer in the Electro-Optical Tracking System

Chao Liu, HaoLin Wang, XiaoXia Qiu, Kang Nie, QianWen Duan, and Yao Mao, *Member, IEEE*

***Abstract*—This article presents a Robust Servo Linear Quadratic Regulator (RSLQR) method based on the Linear Extended State Observer (LESO), which solves the problem of optimal tracking control of electro-optical system under disturbance. For the problem that the accuracy of the electro-optical tracking system is reduced due to disturbance and modeling error, the LESO is adopted in this article to obtain and compensate the influence of internal and external disturbances in the controlled object model, so as to improve the disturbance suppression ability of the electro-optical tracking system. Considering the influence of weighting matrix in the RSLQR method on system's dynamic response performance, this article presents a selection criterion of weighting matrix in the RSLQR to meet the performance requirements of closed-loop system. Through simulation analysis and experimental verification, the design method proposed in this article has great reference value for the optimization of the dynamic response performance of the electro-optical tracking system and the improvement of the disturbance suppression ability.**

***Index Terms*—LESO RSLQR disturbance suppression ability dynamic response performance electro-optical tracking system.**

Manuscript received 28 August 2023; revised 4 January 2024; accepted 17 January 2024. Date of publication 22 January 2024; date of current version 19 February 2024. This work was supported by the National Natural Science Foundation of China under Grant 61905253. *(Corresponding author: Yao Mao.)*

Chao Liu is with the National Key Laboratory of Optical Field Manipulation Science and Technology, Chinese Academy of Sciences, Chengdu 610209, China, also with the Key Laboratory of Optical Engineering, Chinese Academy of Sciences, Chengdu 610209, China, also with the Institute of Optics and Electronics, Chinese Academy of Sciences, Chengdu 610209, China, also with the University of Chinese Academy of Sciences, Beijing 100049, China, and also with the The School of Electronics, Electrical and Communication Engineering, Beijing 100049, China (e-mail: 3229434271@qq.com).

HaoLin Wang and Yao Mao are with the National Key Laboratory of Optical Field Manipulation Science and Technology, Chinese Academy of Sciences, Chengdu 610209, China, also with the Key Laboratory of Optical Engineering, Chinese Academy of Sciences, Chengdu 610209, China, also with the Institute of Optics and Electronics, Chinese Academy of Sciences, Chengdu 610209, China, and also with the University of Chinese Academy of Sciences, Beijing 100049, China (e-mail: iewanghaolin@163.comv; maoyao@ioe.ac.cn).

XiaoXia Qiu is with the National Key Laboratory of Optical Field Manipulation Science and Technology, Chinese Academy of Sciences, Beijing 100045, China, also with the Institute of Optics and Electronics, Chinese Academy of Sciences, Chengdu 610209, China, and also with the University of Chinese Academy of Sciences, Beijing 100049, China (e-mail: 3162383045@qq.com).

Kang Nie and QianWen Duan are with the National Key Laboratory of Optical Field Manipulation Science and Technology, Chinese Academy of Sciences, Beijing 100045, China, also with the Key Laboratory of Optical Engineering, Chinese Academy of Sciences, Chengdu 610209, China, and also with the Institute of Optics and Electronics, Chinese Academy of Sciences, Chengdu 610209, China (e-mail: kangnie@outlook.com; duanqianwen16@mails.ucas.ac.cn).

Digital Object Identifier 10.1109/JPHOT.2024.3356581

I. Introduction

THE electro-optical tracking platform is a kind of complex high-precision directional tracking system integrating light, machine and electricity. It is widely used in the fields of sea, land and air [1], [2], [3]. And it is mainly used for real-time accurate tracking and measurement of moving targets [4], [5]. However, in practical engineering applications, the modeling error and uncertain disturbance of the electro-optical tracking system will cause the tracking accuracy and stability accuracy to decrease. To achieve stable tracking of maneuvering target, two main problems need to be solved: one is how to ensure the stability of optical axis, and the other is target tracking technology [6]. Stability is a prerequisite for tracking. Therefore, better disturbance suppression ability of the platform is conducive to improving the tracking accuracy of the system. At present, most electro-optical tracking platforms use multi-closed-loop control methods, especially three-closed-loop feedback control method, to improve the disturbance suppression ability of the system [7]. However, this method is not designed to suppress the disturbance. And, additional inertial sensors need to be installed on the electro-optical tracking platform, which is not conducive to the characteristics of low inertia and fast speed of the platform, and also increases the space and economic costs. To solve this problem, Deng Chao introduced disturbance observer into the acceleration circuit to improve the disturbance suppression ability of the system [8]. There are two main design methods of disturbance observer. One uses inverse models and low-pass filters. And, the other uses model estimation and high-pass filters. If the observer uses a nominal inverse model, it will inevitably include differential elements, which will amplify the noise and thus affect the robustness and control accuracy of the system [9], [10]. Therefore, it is particularly important to use high-performance control algorithms to enhance the disturbance suppression ability of the electro-optical tracking platform when the hardware conditions of the platform cannot be changed. To solve this problem, Han Jingqing Professor proposed an active disturbance rejection control (ADRC) method independent of the controlled object model, which has a wide application prospect in practical engineering [11]. However, the proposed ADRC method based on nonlinear function has many parameters and complicated adjustment, so it is difficult to achieve simply and fastly control goal in practical application. On the basis of a deep understanding of Han Jingqing's idea

of disturbance suppression, Dr.Gao Zhiqiang correlated a set of ADRC parameters with controller frequency and observer frequency [12]. A large number of simulation experiments and researches prove that the controller with good performance can be obtained by using linear function. And, the calculation of parameter setting is greatly reduced, which is more suitable for engineering application. The linear extended state observer (LESO) expands the total disturbance into a new state variable of the system, and then reconstructs all the states containing the original state variables and the disturbance by using the input and output of the system [13], [14], [15]. This can solve the problem that the accuracy of electro-optical tracking system decreases under disturbance.

On the basis of ensuring that the electro-optical tracking platform has good disturbance suppression ability, the next step is to improve the tracking performance of the system. However, there are few literatures [16] on the optimal tracking control of electro-optical tracking system under disturbance. In practical applications, the electro-optical tracking system not only needs to track the desired trajectory, but also must meet certain control performance indicators, such as minimum tracking time and minimum cost. At present, various optimal control methods are popular in the control field, including linear quadratic optimal control (LQR), adaptive control, neural network control, sliding mode control, etc., to achieve the ideal dynamic and steady state performance [17], [18], [19]. LQR control method is used to design the linear optimal controller. The LQR method can control the tradeoff between system state and control energy well by choosing weighting matrix. Meanwhile, the optimal control law obtained by LQR method has many excellent properties, including closed-loop stability and robustness [20], [21]. This excellent property makes it widely used in engineering applications. However, the influence of weighting matrix selection in LQR method on the closed-loop performance of the system cannot be ignored. In [22] and [23], although a combination of ESO and LQR is proposed to solve the uncertain perturbation problem, the weighting matrix in LQR is selected by the designer according to experience and experimental methods. This method is not only time-consuming and laborious, but also requires high accuracy of the model.

To solve the problems in the ADRC method and LQR method mentioned above, this article develops a strategy to optimize the ADRC method, which uses LQR technology to ensure some closed-loop specifications. On this basis, the input-output behavior of the electro-optical tracking system is approximated by the second-order uncertainty model. And, the linear optimal controller parameters and the related LESO parameters are determined by the LQR method under the modeling error and uncertain disturbance conditions. In addition, a criterion for selecting the weight matrix in the RSLQR method is proposed to ensure that the closed-loop response of the system meets the desired performance. In summary, the contribution of this article is as follows.

i) This article proposes the RSLQR control method based on LESO, which solves the problem of optimal tracking control of electro-optical system under disturbance;

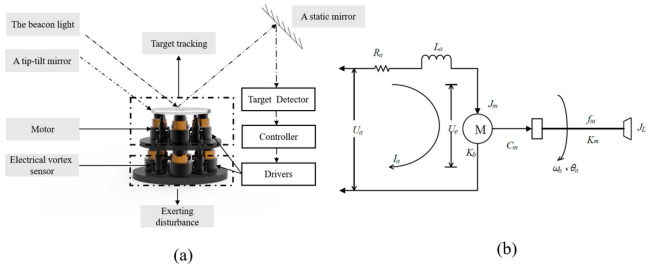

Fig. 1. (a) The schematic of the electro-optical tracking system. (b) The physical model structure of the plant.

ii) In this article, LESO method is used to solve the problem that the accuracy of the electro-optical tracking system decreases under disturbance. And, the stability of the closed-loop system is proved.

iii) The weighting matrix in RSLQR method is very important to the system performance. In this article, the selection of weighting matrix is solved according to the performance requirements of closed-loop system. And, the dynamic response performance of electro-optical tracking system is improved successfully.

The rest of the article is organized as follows. In Section II, the electro-optical tracking platform is modeled. In Section III, the LESO Observer is designed. In Section IV, the RSLQR controller based on LESO are presented and the stability of the closed loop system is discussed. In Sections V and VI, the simulated and experimental results are presented. Finally, the conclusion and future works is given.

II. Modeling of the Electro-Optical Tracking System

Fig. 1(a) shows the controlled object of the precision stability platform, which is often installed in different electro-optical tracking systems for precision stability control. To control the light beam on the platform to remain stable in the Position Sensitivity Detector (PSD), two-axis motion control is carried out by controlling the drive motor, which is usually selected as a voice coil motor to ensure that the precision stable platform has fast response and good linearity control characteristics. Taking one of the axes as an example, the "push and pull" motion mode is realized by the orthogonally mounted voice coil motor, so that the stable platform can carry out a more balanced angular displacement deflection in the direction of the axis. The internal center of the stable platform is connected to the base through a flexible support structure. The control structure has the advantages of no friction, little damping, little inertia and good balance. Therefore, a simplified analysis of its motion model was carried out, and the physical motion model of the platform was obtained, as shown in Fig. 1(b). Based on the armature voltage balance equation and motor torque balance equation, the low-order model characteristics of the stable platform are derived as

$$\begin{cases} U_a = R_a I_a(s) + L_a s I_a(s) + K_b s \theta_a(s) \\ C_m I_a = (J_L s^2 + f_m s + K_m)\theta_a(s) \end{cases}, \quad (1)$$

where $U_a, I_a, R_a, L_a, K_b, C_m, f_m, K_m$ are the motor voltage, current, resistance, inductor, back electromotive force coefficient, torque coefficient, viscous friction and spring stiffness, respectively. Meanwhile, J_L, θ_a are the load inertia and the relative position angle of the motor-driven tilt mirror, respectively.

Then, the controlled system plant can be modeled as

$$G(s) = \frac{\theta_a(s)}{U_a(s)} = \frac{C_m}{(J_L s^2 + f_m s + K_m)(L_a s + R_a) + K_b C_m s}. \tag{2}$$

Therefore, the frequency characteristics of the platform model are characterized as a third-order system. The transfer function molecule in (2) is constant: voltage as input and angular position as output are proportional in physical dimension.Moreover, (2) can be further simplified into the typical resonance element and inertia element. Considering that the mechanical part of the stable platform can be regarded as a single degree of freedom spring torsional vibration system, the transfer relationship between the angular displacement θ_a and the motor torque is a second-order oscillation link, which is represented by the low-order resonance characteristics of the platform. The electrical part of the drive motor is an RL circuit, which is a typical first-order inertial link. In addition, this is only a simple analysis of the low-order characteristics of the platform and there are many high-order resonance links in the high-frequency range, which are temporarily regarded as unmodeled dynamics. Therefore, the position open loop object characteristics of the precision stabilized platform are

$$G(s) = \frac{\theta_a(s)}{U_a(s)} = \frac{K}{(s^2 + as + b)} \frac{1}{(Ts + 1)}, \tag{3}$$

where $a = 2\zeta_{ol}\omega_{ol}, b = \omega_{ol}^2$. ζ_{ol}, ω_{ol} are the damping ratio and natural frequency of the open-loop system, respectively. K is the system open-loop gain. And T is the parasitic time constant.

Since the inertia element in the controlled plant only affects the characteristics of the high-frequency part of the electro-optical tracking platform, the frequency characteristics from the voltage input U_a to the angle output θ_a can be approximated to a typical resonance element. Therefore, the general form of the controlled system object for low frequencies can be expressed as

$$G(s) = \frac{\theta_a(s)}{U_a(s)} = \frac{K}{s^2 + as + b}, \tag{4}$$

where the meanings of a, b and K are consistent with those in (3).

III. The LESO Observer Design

A. Observer Design

The LESO is the core component of linear ADRC. By introducing the concept of extended state, the total disturbance outside the integral series standard form is expanded into a new state variable. The input and output signals of the system are used to reconstruct all system states except the original state variables and the extended state variables. And, the total disturbance is estimated and compensated in real time through feedback control of the original state. The LESO observation and compensation block diagram of the second-order plant is shown in Fig. 2.

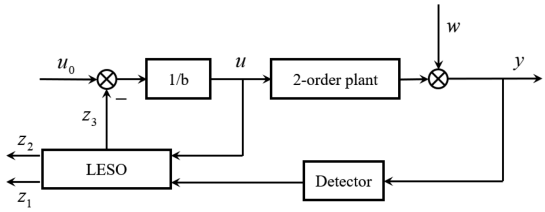

Fig. 2. LESO schematic diagram of the second-order plant.

The second-order plant such as (4) can be expressed as the following differential equation.

$$\ddot{y} = f(y, \dot{y}, w(t), t) + bu \tag{5}$$

where $w(t)$ is the external disturbance and $f(y, \dot{y}, w(t), t)$ is the total disturbance integrating external disturbance and internal disturbance. Selecting the state $x_1 = y, x_2 = \dot{y}, x_3 = f, h = \dot{f}$, (5) can be transformed into the following state equation [24], [25]. x_1, x_2, x_3, h represent the deflection angle, angular velocity, total disturbance of the system and the differential of the total disturbance of the system, respectively.

$$\begin{cases} \dot{\boldsymbol{x}} = \boldsymbol{A}\boldsymbol{x} + \boldsymbol{B}u + \boldsymbol{E}h \\ \boldsymbol{y} = \boldsymbol{C}\boldsymbol{x} \end{cases} \tag{6}$$

where

$$\boldsymbol{A} = \begin{bmatrix} 0 & 1 & 0 \\ 0 & 0 & 1 \\ 0 & 0 & 0 \end{bmatrix}, \boldsymbol{B} = \begin{bmatrix} 0 \\ b \\ 0 \end{bmatrix}, \boldsymbol{C} = [1 \quad 0 \quad 0], \boldsymbol{E} = \begin{bmatrix} 0 \\ 0 \\ 1 \end{bmatrix}. \tag{7}$$

Applying the design of state observer in linear system theory [13], the corresponding continuous LESO equation for a system such as (6) is

$$\begin{aligned} \dot{\boldsymbol{z}} &= [\boldsymbol{A} - \boldsymbol{L}\boldsymbol{C}]\boldsymbol{z} + [\boldsymbol{B}, \boldsymbol{L}]\boldsymbol{u}_{\mathrm{c}} \\ \boldsymbol{y}_{\mathbf{c}} &= \boldsymbol{z}, \end{aligned} \tag{8}$$

where $\boldsymbol{z}$ is the state vector of the observer. And, $\boldsymbol{z}$ observes the state vector of the system such as (6), namely $z_i \approx x_i (i = 1, 2, 3)$. $\boldsymbol{u}_{\mathrm{c}} = [u \quad y]^T$ is the combined input. $\boldsymbol{L}$ is the observer gain matrix, which can be obtained by any known method, such as pole assignment technique,

$$\boldsymbol{L} = \begin{bmatrix} \beta_1 & \beta_2 & \beta_3 \end{bmatrix}^T. \tag{9}$$

When LESO accurately estimates the uncertain disturbance f in a certain frequency range [26], [27], the extended state z_3 is compensated as shown in Fig. 2. The control signal u is

$$u = (u_0 - z_3)/b. \tag{10}$$

By taking (10) into (5), we can get

$$\ddot{y} = b(u_0 - z_3)/b + f(y, \omega, t) \approx u_0. \tag{11}$$

It can be seen that the system is simplified to double integrator series standard type, which makes the design of the control system from complex to simple, from abstract to intuitive.

B. Convergence Analysis

Assuming the error state variable is $e(t) = x(t) - z(t)$. By subtracting (6) from (8), the matrix equation of observation error can be written as

$$\dot{e} = (\boldsymbol{A} - \boldsymbol{LC})e + \boldsymbol{E}\dot{f}. \tag{12}$$

It can be seen that $(\boldsymbol{A} - \boldsymbol{LC})$ determines the eigenvalues of the closed-loop system in the observer error matrix equation. The LESO is bounded-input bounded-output (BIBO) stable if the $(\boldsymbol{A} - \boldsymbol{LC})$ is Hurwitz and f is bounded [28]. Therefore, the roots of the characteristic polynomial of $(\boldsymbol{A} - \boldsymbol{LC})$ are all in the left half plane at $-w_0$,

$$|s\boldsymbol{I} - (\boldsymbol{A} - \boldsymbol{LC})| = (s + \omega_o)^3. \tag{13}$$

By taking (9) and (30) into (13), we get

$$\beta_1 = 3w_0, \beta_2 = 3{w_0}^2, \beta_3 = {w_0}^3. \tag{14}$$

The observer bandwidth w_0 is the only tuning parameter. The proof of these theories in LESO has been given in References [27], [28]. When the uncertainty f or its derivative $\dot{f}$ is bounded, the estimation error is bounded. The upper bound of the estimation error monotonously decreases with the observer bandwidth. If the $\dot{f}$ is globally Lipschitz with respect to x, the dynamic system describing the estimation error is asymptotically stable.

IV. Controller Design

A. The RSLQR Controller

For the controlled plant such as (4), its linear state space equation is expressed as

$$\begin{cases} \dot{\hat{\boldsymbol{x}}} = \hat{\boldsymbol{A}}\hat{\boldsymbol{x}} + \hat{\boldsymbol{B}}\hat{u} \\ \hat{y} = \hat{\boldsymbol{C}}\hat{\boldsymbol{x}} \end{cases}, \tag{15}$$

where $\hat{\boldsymbol{A}}, \hat{\boldsymbol{B}}, \hat{\boldsymbol{x}}$ are the state transition matrix, control matrix and state matrix, respectively. $\hat{y}$ is the output vector and $\hat{\boldsymbol{C}}$ is the corresponding transition matrix.

Based on LQR method, RSLQR method introduces state deviation to form a new broad system matrix, so that the closed-loop system can be stable and the input commands can be tracked accurately [23]. Supposing the error is $e(t) = r(t) - \hat{y}(t)$, where $r(t)$ is the reference signal. In this way, the new state-space equation is expressed as

$$\dot{\boldsymbol{z}} = \tilde{\boldsymbol{A}}\boldsymbol{z} + \tilde{\boldsymbol{B}}\hat{u} + \tilde{\boldsymbol{C}}r, \tag{16}$$

where

$\boldsymbol{z} = [\hat{\boldsymbol{x}} \quad \int e dt]^T, \tilde{\boldsymbol{A}} = \begin{bmatrix} \hat{\boldsymbol{A}} & 0 \\ -\hat{\boldsymbol{C}} & 0 \end{bmatrix}, \tilde{\boldsymbol{B}} = \begin{bmatrix} \hat{\boldsymbol{B}} \\ 0 \end{bmatrix}$ and $\tilde{\boldsymbol{C}} = \begin{bmatrix} \boldsymbol{0} \\ 1 \end{bmatrix}$.

The quadratic cost function of the new system [23] is

$$J = \int_0^\infty \left(\boldsymbol{z}^T(t)\boldsymbol{Q}\boldsymbol{z}(t) + \hat{u}^T(t)\boldsymbol{R}\hat{u}(t)\right)dt, \tag{17}$$

where $\boldsymbol{Q}$ is the semi positive definite state weighting matrix, $\boldsymbol{R}$ is the positive definite control weighting matrix. The performance requirements of the control design are met by selecting the weighting matrix. Generally, the matrix $\boldsymbol{R}$ is selected as the fixed matrix. And, the matrix $\boldsymbol{Q}$ is selected as the diagonal matrix. The gain matrix of the RSLQR control [29] can be expressed as

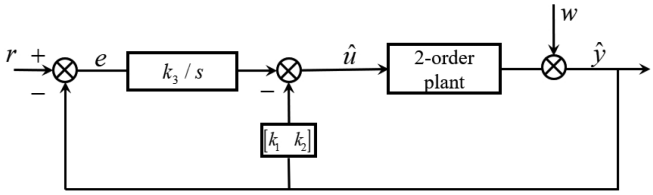

Fig. 3. Schematic diagram of the RSLQR control.

$$\boldsymbol{K_c} = \begin{bmatrix} K_1 & K_2 & K_3 \end{bmatrix} = \boldsymbol{R}^{-1}\tilde{\boldsymbol{B}}^T\boldsymbol{P}, \tag{18}$$

where $\boldsymbol{P}$ is the symmetric positive definite Riccati coefficient matrix which can be obtained by solving continuous algebraic Riccati equation [30]

$$\tilde{\boldsymbol{A}}^T\boldsymbol{P} + \boldsymbol{P}\tilde{\boldsymbol{A}} + \boldsymbol{Q} - \boldsymbol{P}\tilde{\boldsymbol{B}}\boldsymbol{R}^{-1}\tilde{\boldsymbol{B}}^T\boldsymbol{P} = \boldsymbol{0}. \tag{19}$$

The optimal control input of RSLQR control is shown in (18). It can be seen that the RSLQR control method can improve the type of the system and enhance the disturbance suppression ability of the system because of the integration element added to the state feedback control loop. And, the schematic diagram of RSLQR state feedback control is shown in Fig. 3.

$$\hat{u}(t) = -\boldsymbol{K_c}\boldsymbol{z} = -\begin{bmatrix} K_1 & K_2 \end{bmatrix}\hat{\boldsymbol{x}} - K_3\int e\, dt \tag{20}$$

For the controlled system as shown in (4), we define $\hat{x}_1(t) = \hat{y}, \hat{x}_2(t) = \dot{\hat{y}}, \hat{x}_3(t) = \int e(t)dt$. $\hat{x}_1(t), \hat{x}_2(t), \hat{x}_3(t)$ represent the position, velocity and integral of the tracking error of the controlled plant, respectively. The state space method of the controlled plant is modeled as

$$\begin{bmatrix} \dot{\hat{x}}_1(t) \\ \dot{\hat{x}}_2(t) \\ \dot{\hat{x}}_3(t) \end{bmatrix} = \begin{bmatrix} 0 & 1 & 0 \\ -b & -a & 0 \\ -1 & 0 & 0 \end{bmatrix}\begin{bmatrix} \hat{x}_1(t) \\ \hat{x}_2(t) \\ \hat{x}_3(t) \end{bmatrix} + \begin{bmatrix} 0 \\ K \\ 0 \end{bmatrix}\hat{u}(t) + \begin{bmatrix} 0 \\ 0 \\ 1 \end{bmatrix} r, \tag{21}$$

where

$$\tilde{\boldsymbol{A}} = \begin{bmatrix} 0 & 1 & 0 \\ -b & -a & 0 \\ -1 & 0 & 0 \end{bmatrix}, \quad \tilde{\boldsymbol{B}} = \begin{bmatrix} 0 \\ K \\ 0 \end{bmatrix}. \tag{22}$$

In optimal control, the standard practice is to design the regulator by changing the value of the weighting matrix $\boldsymbol{Q}$ and keeping the weighting matrix $\boldsymbol{R}$ constant. We assume that the correlation weighting matrices $\boldsymbol{Q}$, $\boldsymbol{R}$ and $\boldsymbol{P}$ are

$$\boldsymbol{Q} = \begin{bmatrix} q_1 & 0 & 0 \\ 0 & q_2 & 0 \\ 0 & 0 & q_3 \end{bmatrix}, \boldsymbol{R} = [\gamma], \boldsymbol{P} = \begin{bmatrix} p_{11} & p_{12} & p_{13} \\ p_{12} & p_{22} & p_{23} \\ p_{13} & p_{23} & p_{33} \end{bmatrix}. \tag{23}$$

By taking (20) and (21) into (16), we can get

$$K_1 = \gamma^{-1}Kp_{12}, K_2 = \gamma^{-1}Kp_{22}, K_3 = \gamma^{-1}Kp_{23}. \tag{24}$$

The corresponding closed-loop system matrix $\boldsymbol{A_c} = \tilde{\boldsymbol{A}} - \tilde{\boldsymbol{B}}\boldsymbol{R}^{-1}\tilde{\boldsymbol{B}}^T\boldsymbol{P}$ is

$$\boldsymbol{A_c} = \begin{bmatrix} 0 & 1 & 0 \\ -b - \eta p_{12} & -a - \eta p_{22} & -\eta p_{23} \\ -1 & 0 & 0 \end{bmatrix}, \tag{25}$$

where η is $\gamma^{-1}K^2$.

Therefore, the closed-loop system characteristic equation $\Delta(s) = |s\boldsymbol{I} - \boldsymbol{A_c}|$ is

$$\Delta(s) = s^3 + (a + \eta p_{22})\, s^2 + (b + \eta p_{12})\, s - \eta p_{23}. \quad (26)$$

Since the closed-loop system matrix obtained by (23) does not contain any time delay, the method of pole configuration is directly applied to obtain the desired closed-loop performance. The matrix $\boldsymbol{A_c}$ can be determined by setting the characteristic equation of the closed-loop system $\Delta(s)$ equal to the desired closed-loop equation.

When $\boldsymbol{A_c}$ is a 2×2 matrix, the closed-loop system characteristic equation $\Delta(s)$ is

$$\Delta(s) = (s + p_1)(s + p_2) = s^2 + 2s\zeta_{cl}\omega_{cl} + \omega_{cl}^2, \quad (27)$$

where

$p_1 = \zeta_{cl}\omega_{cl} + i\omega_{cl}\sqrt{1-\zeta_{cl}^2}$, $p_2 = \zeta_{cl}\omega_{cl} - i\omega_{cl}\sqrt{1-\zeta_{cl}^2}$, with ζ_{cl} and ω_{cl} as the desired closed-loop damping ratio and natural frequency.

When $\boldsymbol{A_c}$ is a 3×3 matrix, using the dominant pole placement method, the closed-loop system characteristic equation $\Delta(s)$ is

$$\begin{aligned}\Delta(s) &= (s + p_1)(s + p_2)(s + p_3) \\ &= (s + m\zeta_{cl}\omega_{cl})\left(s^2 + 2s\zeta_{cl}\omega_{cl} + \omega_{cl}^2\right) \end{aligned} \quad (28)$$

where the location of non-dominant pole $p_3 = m\zeta_{cl}\omega_{cl}$ is placed m times away from the real part of the dominant closed-loop poles. Meanwhile, $m \gg \zeta_{cl}\omega_{cl}$, which ensures that the closed-loop pole is at the dominant pole position [31]. We call this m as the relative dominance and as per the literature [21] its value should be chosen around 3 or more.

Comparing the coefficients before the same state variables on the right side of (24) and (26), we can get

$$\begin{aligned} p_{12} &= \frac{\omega_{cl}^2 + 2m\zeta_{cl}^2\omega_{cl}^2 - b}{\eta}, \\ p_{22} &= \frac{(2+m)\zeta_{cl}\omega_{cl} - a}{\eta}, \\ p_{23} &= \frac{-m\zeta_{cl}\omega_{cl}^3}{\eta}. \end{aligned} \quad (29)$$

The remaining elements of the matrices $\boldsymbol{P}$ and $\boldsymbol{Q}$ can be obtained by solving the Riccati equation in (17).

$$\begin{aligned} q_1 &= \eta p_{12}^2 + 2bp_{12} + 2p_{13} \\ q_2 &= \eta p_{22}^2 + 2ap_{22} - 2p_{12} \\ q_3 &= \eta p_{23}^2 \\ p_{11} &= \eta p_{12}p_{22} + ap_{12} + bp_{22} + p_{23} \\ p_{13} &= \eta p_{22}p_{23} + ap_{23} \\ p_{33} &= -bp_{23} - \eta p_{12}p_{23} \end{aligned} \quad (30)$$

B. The RSLQR Controller Based on LESO

Since the integral element is introduced into RSLQR method, the dynamic response performance and disturbance suppression ability of the electro-optical tracking system can be improved well. In other words, the RSLQR method improves the type of the system. Next, on the premise of maintaining the advantages of the dynamic response of the system under the RSLQR method, the introduction of LESO into the system is considered to further solve the problem of the system precision decline under the disturbance.

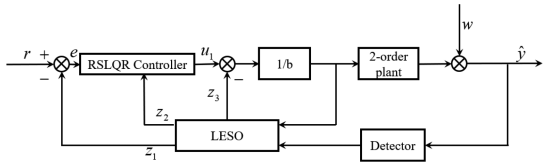

Fig. 4. Schematic diagram of the RSLQR controller based on LESO.

For the LESO observer design in Section III, the system will be simplified as a double integral standard form, i.e.$\ddot{\hat{y}} = u_1$ in Fig. 4. And, the state space of the controlled plant is modeled as

$$\begin{bmatrix}\dot{x}_1(t)\\ \dot{x}_2(t)\\ \dot{x}_3(t)\end{bmatrix} = \begin{bmatrix}0 & 1 & 0\\ 0 & 0 & 0\\ -1 & 0 & 0\end{bmatrix}\begin{bmatrix}x_1(t)\\ x_2(t)\\ x_3(t)\end{bmatrix} + \begin{bmatrix}0\\ 1\\ 0\end{bmatrix} u_1(t) + \begin{bmatrix}0\\ 0\\ 1\end{bmatrix} r, \quad (31)$$

where $\hat{x}_1(t) = \hat{y}, \hat{x}_2(t) = \dot{\hat{y}}, \hat{x}_3(t) = \int e(t)dt$.

Assuming that the correlation weighting matrices $\boldsymbol{Q}$, $\boldsymbol{R}$ and $\boldsymbol{P}$ are consistent with (21). By taking (21) and (29) into (16), we can get

$$K_1 = \gamma^{-1}p_{12}, K_2 = \gamma^{-1}p_{22}, K_3 = \gamma^{-1}p_{23}. \quad (32)$$

The closed-loop system characteristic equation $\Delta(s)$ is

$$\Delta(s) = s^3 + \gamma^{-1}p_{22}s^2 + \gamma^{-1}p_{12}s - \gamma^{-1}p_{23}. \quad (33)$$

By comparing the coefficients before the same state variable on the right side of (31) and (26), we can get

$$\begin{aligned} p_{12} &= \frac{\omega_{cl}^2 + 2m\zeta_{cl}^2\omega_{cl}^2}{\gamma^{-1}}, \\ p_{22} &= \frac{(2+m)\zeta_{cl}\omega_{cl}}{\gamma^{-1}}, \\ p_{23} &= \frac{m\zeta_{cl}\omega_{cl}^3}{-\gamma^{-1}}. \end{aligned} \quad (34)$$

The remaining elements of the matrices $\boldsymbol{P}$ and $\boldsymbol{Q}$ can be obtained by solving the Riccati equation in (17).

$$\begin{aligned} q_1 &= \gamma^{-1}p_{12}^2 + 2p_{13} \\ q_2 &= \gamma^{-1}p_{22}^2 - 2p_{12} \\ q_3 &= \gamma^{-1}p_{23}^2 \\ p_{11} &= \gamma^{-1}p_{12}p_{22} + p_{23} \\ p_{13} &= \gamma^{-1}p_{22}p_{23} \\ p_{33} &= -\gamma^{-1}p_{12}p_{23} \end{aligned} \quad (35)$$

C. Closed-Loop Stability Analysis

On the basis of LESO convergence, the stability analysis process of closed-loop control system is given. The stability

analysis refers to BIBO stability, that is, bounded input produces bounded output.

For the following system

$$y^n(t) = f\left(y^{n-1}(t), y^{n-2}(t), \ldots, y(t), w(t)\right) + bu(t), \quad (36)$$

where $y(t)$ indicates the output of the controlled object; $w(t)$ is the external unknown disturbance; $u(t)$ indicates the input of the controlled object; b is the input amplification constant; $f(y^{n-1}(t), y^{n-2}(t), \ldots, y(t), w(t))$ is the total disturbance of the system. Assuming $\dot{f} = h$, the new extended state variable x_{n+1} is introduced into the above n-order system to obtain all state variables $x = [\ x_1 \quad x_2 \quad \cdots \quad x_n \quad x_{n+1}\ ]^T$.

Rewrite the system in (36) into the following extended state space form:

$$\begin{aligned} \dot{x} &= Ax + Bu + Eh \\ y &= Cx, \end{aligned} \quad (37)$$

where $A = \begin{bmatrix} 0 & 1 & 0 & \cdots & 0 \\ 0 & 0 & 1 & \cdots & 0 \\ \vdots & \vdots & \vdots & \ddots & \vdots \\ 0 & 0 & 0 & \cdots & 1 \\ 0 & 0 & 0 & \cdots & 0 \end{bmatrix}, B = \begin{bmatrix} 0 \\ 0 \\ \vdots \\ b \\ 0 \end{bmatrix}, C = \begin{bmatrix} 1 & 0 & \cdots & 0 & 0 \end{bmatrix}, E = \begin{bmatrix} 0 \\ 0 \\ \vdots \\ 0 \\ 1 \end{bmatrix}$.

For the extended state system shown in (37), LESO is designed as

$$\begin{aligned} \dot{z} &= [A - LC]\, z + [B, L]\, u_l \\ y_l &= z, \end{aligned} \quad (38)$$

where $z = [z_1 \quad z_2 \quad \cdots \quad z_n \quad z_{n+1}]^T$ is the state vector of LESO. The combined input of LESO is the control input and output of the system, i.e $u_l = [\ u \quad y\ ]^T$. The output y_l of LESO is the state vector z. $L = [\ \beta_1 \quad \beta_2 \quad \cdots \quad \beta_n \quad \beta_{n+1}\ ]^T$ is the observer gain matrix designed for LESO.

Given the bounded reference input r of the system, the control law generated [24], [25] from LESO observation vector z is

$$u = \frac{k_1}{b}(r - z_1) + \cdots + \frac{k_n}{b}(r^{n-1} - z_n) + \frac{1}{b}(r^n - z_{n+1}), \quad (39)$$

where $K = [k_1 \quad k_2 \quad \cdots \quad k_{n-1} \quad k_n]$ is the controller parameters to be determined. Assuming $r_1 = r, r_2 = \dot{r}, \cdots r_{n+1} = r^n$, we get

$$\begin{cases} \dot{e}_1 = \dot{r}_1 - \dot{x}_1 \\ \vdots \\ \dot{e}_{n-1} = \dot{r}_{n-1} - \dot{x}_{n-1} = e_n \\ \dot{e}_n = \dot{r}_n - \dot{x}_n = r_{n+1} - y^n \\ = -k_1 e_1 - \cdots - k_n e_n - k_1 \hat{e}_1 - \cdots - k_n \hat{e}_n \end{cases}, \quad (40)$$

where $e_i = r_i - x_i (i = 1, \ldots, n)$ is the $(i-1)$-order differential value of the system tracking error; $\hat{e}_i = x_i - z_i (i = 1, \cdots n+1)$ is observation error of the system.

Let $e = [\ e_1 \quad \cdots \quad e_{n-1} \quad e_n\ ]^T, \hat{e} = [\ \hat{e}_1 \quad \cdots \quad \hat{e}_{n-1} \quad \hat{e}_n\ ]^T$,

$$A_{11} = \begin{bmatrix} 0 & 1 & \cdots & 0 & 0 \\ 0 & 0 & \cdots & 0 & 0 \\ \vdots & \vdots & \ddots & \vdots & \vdots \\ 0 & 0 & \cdots & 0 & 1 \\ -k_1 & -k_2 & \cdots & -k_{n-1} & -k_n \end{bmatrix}, \text{ and}$$

$$A_{22} = \begin{bmatrix} 0 & 0 & \cdots & 0 & 0 \\ 0 & 0 & \cdots & 0 & 0 \\ \vdots & \vdots & \ddots & \vdots & \vdots \\ 0 & 0 & \cdots & 0 & 0 \\ -k_1 & -k_2 & \cdots & -k_{n-1} & -k_n \end{bmatrix},$$

we can rewrite (40) as

$$\dot{e} = A_{11} e + A_{22} \hat{e}. \quad (41)$$

By solving (41), we can get

$$e(t) = e^{A_{11} t} e(0) + \int_0^t e^{A_{11}(t-\tau)} A_{22} \hat{e}(\tau) d\tau. \quad (42)$$

According to (41), $\forall t \geq T_1$

$$[A_{22}\hat{e}(\tau)] = 0, (i = 1, \ldots, n-1), \quad (43)$$

$$|[A_{22}\hat{e}(\tau)]|_n = |-k_1\hat{e}_1(\tau) - \cdots - k_n\hat{e}_n(\tau)| \leq k_s M_1 = \eta, \quad (44)$$

where $k_s = 1 + \sum_{i=1}^n k_i$. M_1 mentioned in the relevant literature [27], [28].

Let $\varphi(t) = \int_0^t e^{A_{11}(t-\tau)} A_{22}\hat{e}(\tau) d\tau, \psi = [\ 0 \quad \cdots \quad 0 \quad \gamma\ ]^T$, we can get

$$\begin{aligned} |\varphi_i(t)| &= \int_0^t \left[e^{A_{11}(t-\tau)} A_{22}\hat{e}(\tau)\right]_i d\tau \leq \int_0^t \left[e^{A_{11}(t-\tau)}\psi\right]_i d\tau \\ &\leq \left|(A_2^{-1}\psi)_i\right| + \left|(A_2^{-1} e^{A_{11} t}\psi)_i\right|, \end{aligned} \quad (45)$$

where $i = 1, \ldots, n, A_{11}^{-1} = \begin{bmatrix} -\frac{k_2}{k_1} & -\frac{k_3}{k_1} & \cdots & -\frac{k_n}{k_1} & -\frac{1}{k_1} \\ 1 & 0 & \cdots & 0 & 0 \\ 0 & 1 & \cdots & 0 & 0 \\ \vdots & \vdots & \ddots & \vdots & \vdots \\ 0 & 0 & \cdots & 1 & 0 \end{bmatrix}$,

$|(A_{11}^{-1}\psi)_i| = \begin{cases} \frac{\gamma}{k_1} = \frac{\gamma}{w_c^n}, (i = 1) \\ 0, (i = 2, \ldots, n) \end{cases}$

Since A_{11} is Hurwitz, there is a bounded time $T_2 > 0$, that is, $\forall t \geq T_2 > 0$ the following relation is satisfied.

$$\left|\left[e^{A_{11} t}\right]_{ij}\right| \leq \frac{1}{w_c^{n+1}}, \quad (46)$$

where $i, j = 1, \ldots, n$. Particularly, the value of T_2 depends on A_{11}.

Let $e^{A_{11} t} = \begin{bmatrix} c_{11} & \cdots & c_{1n} \\ \vdots & \ddots & \vdots \\ c_{n1} & \cdots & c_{nn} \end{bmatrix}, e_s(0) = |e_1(0)| + |e_2(0)| + \cdots |e_n(0)|$, we can get

$$\begin{aligned} &\left|\left[e^{A_{11} t} e(0)\right]_i\right| = |c_{i1}e_1(0) + c_{i2}e_2(0) + \cdots + c_{in}e_n(0)| \\ &\leq |c_{i1}e_1(0)| + |c_{i2}e_2(0)| + \cdots + |c_{in}e_n(0)| \\ &\leq \frac{|e_1(0)| + |e_2(0)| + \cdots + |e_n(0)|}{w_c^{n+1}} = \frac{e_s(0)}{w_c^{n+1}} \end{aligned} \quad (47)$$

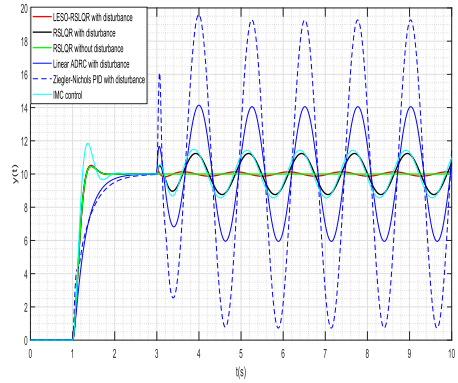

Fig. 5. Comparison of the system step response.

for $\forall t \geq T_2 > 0$, where $i = 1, \ldots, n$.

Let $T_3 = \max\{T_1, T_2\}$, we can get

$$\left|(e^{A_2 t}\psi)_i\right| \leq \frac{\gamma}{w_c^{n+1}}$$

$$\left|(A_2^{-1}e^{A_2 t}\psi)_i\right| \leq \begin{cases} \frac{1+\sum_{i=1}^{n} k_i}{w_c^n}\frac{\gamma}{w_c^n}, (i=1) \\ \frac{\gamma}{w_c^{n+1}}, (i=2,\ldots,n) \end{cases}, \quad (48)$$

for $\forall t \geq T_3$.

By (45) and (48), we can get

$$|\varphi_i(t)| \leq \begin{cases} \frac{1+\sum_{i=2}^{n} k_i}{w_c^n}\frac{\gamma}{w_c^{n+1}} + \frac{\gamma}{w_c^n}, (i=1) \\ \frac{\gamma}{w_c^{n+1}}, (i=2,\ldots,n) \end{cases}. \quad (49)$$

According to (42), it can be obtained:

$$|e_i(t)| \leq \left|\left[e^{A_2 t}e(0)\right]_i\right| + |\varphi_i(t)|. \quad (50)$$

By (47),(49) and (50), we can get

$$|e_i(t)| \leq \begin{cases} \frac{1+\sum_{i=2}^{n} k_i}{w_c^n}\frac{\gamma}{w_c^{n+1}} + \frac{\gamma}{w_c^n} + \frac{e_s(0)}{w_c^{n+1}}, (i=1) \\ \frac{e_s(0)+\gamma}{w_c^{n+1}}, (i=2,\ldots,n) \end{cases} \leq M_2, \quad (51)$$

where $M_2 = \max\left\{\frac{1+\sum_{i=2}^{n} k_i}{w_c^n}\frac{\gamma}{w_c^{n+1}} + \frac{\gamma}{w_c^n} + \frac{e_s(0)}{w_c^{n+1}}, \frac{e_s(0)+\gamma}{w_c^{n+1}}\right\}$.

According to the above proof process, it can be seen that when the observation error of the observer converges, there is a controller that makes the error of the closed-loop system converge within the effective time.

V. Simulation Analysis

For the open-loop object model of the electro-optical tracking platform obtained by the spectrum analyzer, as shown in Fig. 12. The transfer function is

$$G(s) = \frac{1776.4}{s^2 + 25.6\,s + 1421.2}. \quad (52)$$

A. The RSLQR Controller Based on LESO

In the design of RSLQR controller based on LESO, the desired system damping ratio ζ_{cl}, natural frequency ω_{cl} and relative dominance m are taken as $\zeta_{cl} = 1.25, \omega_{cl} = 17, m = 100$. Meanwhile, $m \gg \zeta_{cl}\omega_{cl}$ is satisfied, which ensures that the closed-loop pole is at the dominant pole position. In general, the weighting matrix $\boldsymbol{R} = 1$. Using Eqs.(34) and (35), matrices $\boldsymbol{P}$ and $\boldsymbol{Q}$ can be evaluated as

$$\boldsymbol{P} = \begin{bmatrix} 195764626 & 90601 & -1331115937 \\ 90601 & 2167.5 & -614125 \\ -1331115937 & -614125 & 55640646187 \end{bmatrix},$$

$$\boldsymbol{Q} = \begin{bmatrix} 5546399927 & 0 & 0 \\ 0 & 4516853 & 0 \\ 0 & 0 & 377149515625 \end{bmatrix}. \quad (53)$$

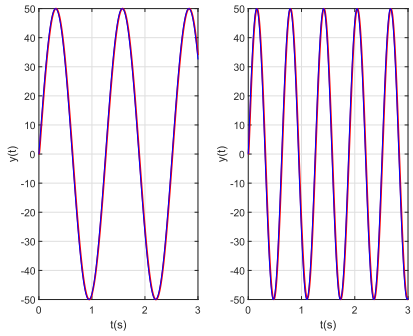

Fig. 6. Estimation of LESO for external disturbance $50\sin(5t)$ and $50\sin(10t)$.

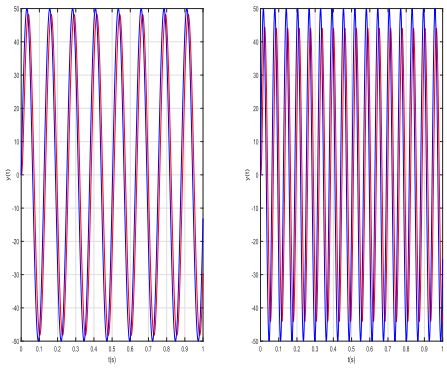

Fig. 7. Estimation of LESO for external disturbance $50\sin(50t)$ and $50\sin(100t)$.

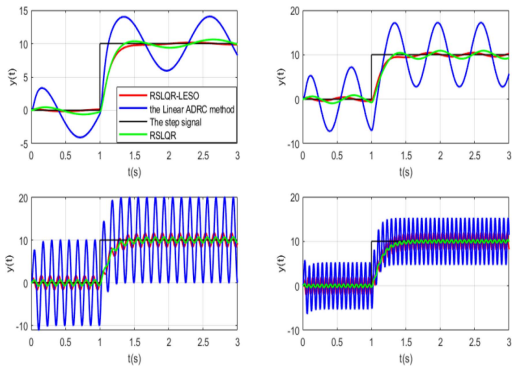

Fig. 8. Comparison of step responses under different methods at the internal and external disturbance such as $50\sin(5t)$, $50\sin(10t)$, $50\sin(50t)$ and $50\sin(100t)$.

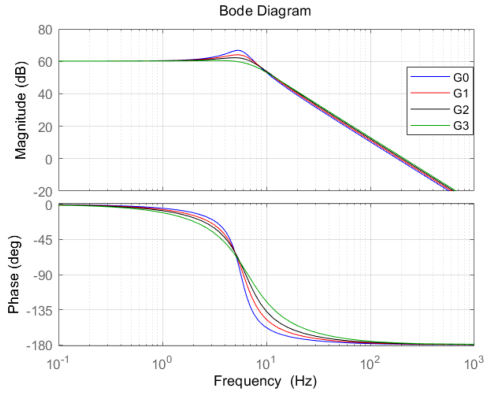

Fig. 9. Characteristics of the controlled plant at different natural frequencies ω_{ol}, damping ratio ζ_{ol} and the open-loop gain K.

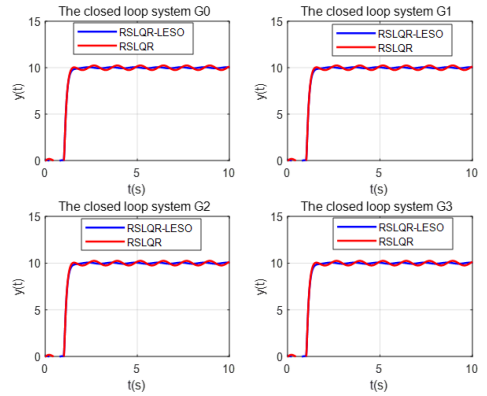

Fig. 10. The Step response of the controlled plant at different natural frequencies ω_{ol}, damping ratio ζ_{ol} and the open-loop gain K.

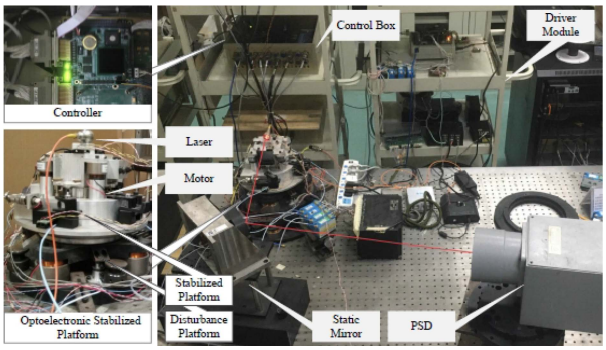

Fig. 11. Electro-optical tracking experimental platform.

The eigen values of matrices $\boldsymbol{P}$ and $\boldsymbol{Q}$ are

$$eig\left[\boldsymbol{P}\right]=\begin{bmatrix}2125.57\\163825743\\55672585112\end{bmatrix}\text{ and }eig\left[\boldsymbol{Q}\right]=\begin{bmatrix}4516853\\5546399927\\377149515625\end{bmatrix}. \tag{54}$$

The positive eigen values of matrices $\boldsymbol{P}$ and $\boldsymbol{Q}$ indicate that the positive definite condition of LQR is satisfied. The RSLQR controller parameters based on LESO are calculated by using

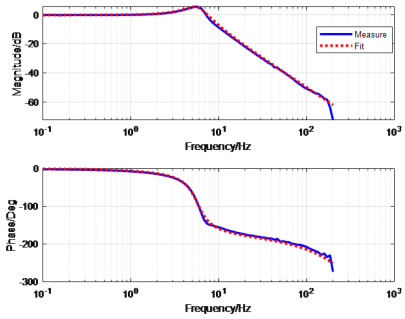

Fig. 12. Characteristic of the controlled plant.

(32) as

$$\begin{bmatrix}K_1 & K_2 & K_3\end{bmatrix}=\begin{bmatrix}90602 & 2167.5 & 614125\end{bmatrix}. \tag{55}$$

Therefore, the RSLQR controller based on LESO is

$$u(t)=-90602x_1-2167.5x_2+614125x_3. \tag{56}$$

As for LESO design, in order to satisfy $w_0 \gg m \gg \zeta_{cl}\omega_{cl}$, the observer bandwidth w_0 is set to 400 in the simulation. By (14), the observer gain parameters $\beta_1, \beta_2, \beta_3$ are

$$\begin{bmatrix}\beta_1 & \beta_2 & \beta_3\end{bmatrix}=\begin{bmatrix}1200 & 480000 & 64000000\end{bmatrix}. \tag{57}$$

B. The Other Control Methods

In the design of the PID controller based on Ziegler-Nichols, the PID controller parameters are $K_p = 0.196, K_i = 2.674, K_d = 0.0036$. To ensure the fairness of the comparison, the observer bandwidth w_0 of the traditional Linear ADRC method is also set at 400 Hz. The traditional Linear ADRC controller and observer are designed and tuned according to the reference [31]. A common rule of thumb is to choose $w_0 = 3 \sim 5w_c$, where w_c is the controller bandwidth of Linear ADRC. The common linear PD control law in Fig. 2 is $u = k_p(r - z_1) - k_d z_2$, where $k_p = {w_c}^2, k_d = 2w_c$.

To verify the effectiveness of LESO method, control group RSLQR method is set up. To ensure the fairness of comparison in the RSLQR method, the desired system damping ratio ζ_{cl}, natural frequency ω_{cl} and relative dominance m are also taken as $\zeta_{cl} = 1.25, \omega_{cl} = 17, m = 100$. Meanwhile, $m \gg \zeta_{cl}\omega_{cl}$ is satisfied, which ensures that the closed-loop pole is at the dominant pole position [31]. The eigenvalues of the tested matrices $\boldsymbol{P}$ and $\boldsymbol{Q}$ are positive, which indicates that the positive definite condition of LQR is also satisfied. By using (24), the RSLQR controller is

$$\hat{u}(t) = -50.2\hat{x}_1 - 1.21\hat{x}_2 + 345.7\hat{x}_3. \tag{58}$$

Fig. 5 shows the comparison of step response of the system under different methods. In the simulation, the external disturbance of $10\sin(5t)$ is applied to the controlled plant at 3 s. The internal disturbance is the a, b, K parameters in (4) change by 40% of the original. It can be seen that the RSLQR control improves the type of the system and enhances the disturbance suppression ability. This is due to the incorporation of an integral element into the state feedback control loop. Therefore, the

RSLQR control can improve the dynamic performance of the system. Specifically, compared with the linear ADRC method, Internal Model Control method [32] (IMC) and the PID controller based on Ziegler-Nichols method, dynamic performance of the system under the RSLQR method such as the risen time, settling time of the system has been significantly improved. Meanwhile, the disturbance suppression ability of the system under the RSLQR method has also been significantly improved. Therefore, the RSLQR method has great advantages. It can also be seen that the RSLQR controller based on LESO in the article significantly improves the dynamic response of the system and the disturbance suppression ability of the system, as shown in the red line in Fig. 5.

The electro-optical tracking platform in the actual working environment not only be affected by external interference, but also its characteristics will change with the change of attitude and load. The external disturbance $50\sin(5t)$, $50\sin(10t)$, $50\sin(50t)$ and $50\sin(100t)$ are applied to the electro-optical tracking platform respectively, as shown in Figs. 6 and 7. Meanwhile, the internal disturbance is also applied to the electro-optical tracking platform. And the internal disturbance is the a, b, K parameters in (4) change by 40% of the original. In Figs. 6 and 7, the blue line represents the actual value of the disturbance. And, the red line represents the estimation of the observer.

Fig. 6 shows that LESO can accurately estimate the given sinusoidal disturbance $50\sin(5t)$ and $50\sin(10t)$, where the observed disturbance amplitude is basically the same as the actual value. Fig. 7 shows that LESO can also estimate the given sinusoidal disturbance $50\sin(50t)$, where the observed disturbance amplitude is almost the same as the actual value, but there is a phase difference between the observed value and the actual value. This may lead to poor disturbance compensation effect of LESO. It can also be seen from Fig. 7 that with the increase of disturbance frequency, there is a certain error in the estimated value of disturbance $50\sin(100t)$.

Fig. 8 shows the response of the system when the controller with and without LESO under different disturbance conditions. When the external disturbance is respectively $50\sin(5t)$ and $50\sin(10t)$, compared with the RSLQR controller, the disturbance suppression ability of the system under the RSLQR controller based on LESO has been significantly improved. However, when the external disturbance is respectively $50\sin(50t)$ and $50\sin(100t)$, the disturbance suppression ability of the system under the RSLQR controller based on LESO has no significantly improved. This result is caused by the error between the observed LESO value and the actual disturbance value, which is consistent with the conclusion in Fig. 7.

Fig. 8 also shows the step response under the linear ADRC method. In the linear ADRC method, observer bandwidth w_0 is also $w_0 = 400$ Hz. Compared with the linear ADRC method, the RSLQR controller based on LESO proposed in this article significantly improves the dynamic property and disturbance suppression ability of the system. The closed-loop performance indexes corresponding to the RSLQR controller based on LESO, the RSLQR controller, IMC method, Z-N PID controller and the linear ADRC method under internal disturbance, such as overshoot percentage $OS\%$, stability time $T_s(s)$ and risen time $T_r(s)$, are shown in Table I for reference and comparison.

TABLE I
CLOSED LOOP PERFORMANCE MEASURES

Method	ζ_{cl}	ω_{cl}	m	$T_r(s)$	$T_s(s)$	$OS\%$
RSLQR-LESO	1.25	17	100	1.31	1.49	0.03
RSLQR	1.25	17	100	1.31	1.49	0.03
linear ADRC	···	···	···	2.14	2.38	0
IMC method	···	···	···	1.44	2.12	0.2
The Z-N PID controller	···	···	···	2.22	2.63	0

In conclusion, the RSLQR controller based on LESO proposed in this article solves the problem of optimal tracking control of electro-optical system under disturbance. Meanwhile, The RSLQR controller based on LESO has a better control effect than the RSLQR controller for uncertain disturbance in a certain frequency range.

C. Robustness Test of the RSLQR Controller Based on LESO

The parameters of the RSLQR controller based on LESO are shown in (55). In the simulation, the influence of the natural frequency ω_{ol}, damping ratio ζ_{ol} and the open-loop gain K of the controlled system on the system robustness is studied, as shown in Figs. 9 and 10.

The Fig. 9 shows that the characteristics of the controlled plant at different natural frequencies ω_{ol}, damping ratio ζ_{ol} and the open-loop gain K, where G1 represents the nominal controlled system. In Fig. 9, G0 represents the controlled plant of natural frequency $\omega_{ol} = 35.7\,Hz$, damping ratio $\zeta_{ol} = 0.24$ and open loop gain $K = 1019.6$; G1 represents the controlled plant of natural frequency $\omega_{ol} = 37.7HZ$, damping ratio $\zeta_{ol} = 0.34$ and open loop gain $K = 1776.6$; G2 represents the controlled plant of natural frequency $\omega_{ol} = 39.7HZ$, damping ratio $\zeta_{ol} = 0.44$ and open loop gain $K = 5122.3$; G3 represents the controlled plant of natural frequency $\omega_{ol} = 41.7HZ$, damping ratio $\zeta_{ol} = 0.64$ and open loop gain $K = 8694.5$.

In Fig. 10, the external disturbance is $20\sin(5t)$. Meanwhile, the natural frequency of the system ω_{ol} changes from $35.7\,Hz$ to $41.7\,Hz$. The damping ratio of the system ζ_{ol} changes from 0.24 to 0.64 and the open-loop gain K changes from 1019.6 to 8694.5. Compared with the RSLQR controller, the system under RSLQR control based on LESO has good robustness. This is because the controller not only estimates the state information of the system, but also obtains the influence of internal and external disturbances in the object model in real-time, and compensates for the control parameters obtained by the RSLQR controller online.

VI. EXPERIMENTAL VERIFICATION

The devices of the electro-optical tracking system are shown in Fig. 11, including light source, stabilization platform, disturbance platform, digital controller box, digital-analog/analog-to-digital converter, power drive amplifier module and Position Sensitivity Detector (PSD). The control box is mainly composed

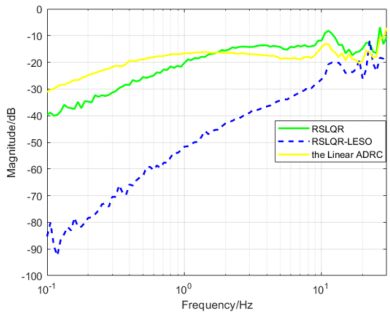

Fig. 13. Disturbance suppression ability (DSA) of the RSLQR controller, the linear ADRC and the RSLQR controller based on LESO.

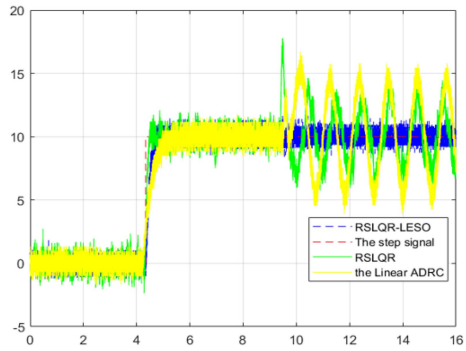

Fig. 14. Comparison of step responses under the different methods.

of digital controller equipped with VxWorks real-time operating system (RTOS), flight board based on field Programmable gate array (FPGA) and MOXA PC/104 serial card.

The enlarged image at the bottom left shows that the stabilization platform is installed above the disturbance platform, the former is used to stabilize the optical axis, and the latter is used to simulate the external complex disturbance sources in the moving carrier environment. The static mirror reflects the optical path into the PSD. And, the beam jitter and the optic axis stability error can be calculated according to the deviation of the center position measured by the detector. In addition, loads of different masses can be installed around the stabilized platform to change the parameter characteristics of the controlled object. At the same time, under the action of disturbance input, the stabilized platform may have coupling disturbances of uneven mass torque and moment of inertia torque under different working states of attitude or Angle, as well as inaccurate and unmodeled parts of its own modeling. These internal and external disturbances jointly affect the optical axis of the stabilized platform. Since the two axes of the stable platform are orthogonal and symmetrical, the single axis is usually used as an example to verify and compare the performance of the control algorithm in the experiment. To quantitatively analyze the disturbance suppression performance of the stable platform, an eddy current sensor is installed on the disturbance platform to measure the disturbance angle position input. In this way, the influence of disturbance input to the final stability error can be obtained under different closed-loop control methods. The angular position signal and error signal are obtained by PSD. And, the angular rate signal is obtained by gyro sensor. The digital controller uses the embedded real-time operating system with sampling frequency of 5 kHz to process the digital signal, execute the control signal instruction and drive the stable platform movement.

The characteristic of the controlled plant is shown in Fig. 12 by inputting the sweep signal to the system, which holds the transfer function (59) by the parameters identification

$$G(s) = \frac{1776.4}{(s^2 + 25.6\mathrm{s} + 1421.2)}. \tag{59}$$

Firstly, the linear ADRC method is applied to the electro-optical tracking experimental platform. And, the disturbance $10\sin(2pit)$ is applied to the disturbance platform. In the linear ADRC method, the observer bandwidth w_0 is 400 Hz and the observer gain parameters were obtained by (14).

Secondly, the RSLQR controller and the RSLQR controller based on LESO are also applied to the electro-optical tracking platform. The RSLQR controller and the RSLQR controller based on LESO are shown in (58) and (56). The disturbance input of the electro-optical tracking experimental platform is the value measured by the sensor on the disturbance platform. So, the DSA is defined as the frequency characteristics from the final stabilization error to the disturbance input. The comparison results of DSA of three methods in the range from $0.1 - 30$ Hz are shown in Fig. 13.

It is seen from Fig. 13 that compared with the controller without LESO, the disturbance suppression ability of the system with LESO is significantly improved in the range of $0.1 - 30$ Hz frequency domain. Meanwhile, compared with the linear ADRC method, the disturbance suppression ability of the system under the RSLQR controller based on LESO is significantly improved. To more clearly reflect the effect of disturbance suppression, the time-domain effect diagram of sinusoidal disturbance suppression at 1 Hz was selected in this experiment, as shown in Fig. 14.

Fig. 14 shows the step response under the RSLQR controller based on LESO. For comparison, the step response under the RSLQR controller and the linear ADRC method are also shown. It is clear that compared with the RSLQR controller, the RSLQR controller based on LESO can significantly improves disturbance suppression ability of the system. Meanwhile, compared with the Linear ADRC method, the RSLQR controller based on LESO can significantly improve the dynamic property and disturbance suppression ability of the system. Therefore, the RSLQR controller based on the LESO proposed in this article has great advantages in the electro-optical tracking control system.

VII. Conclusions and Future Works

In this article, the LESO is used to obtain and compensate the influence of internal and external disturbance in the controlled object model, so as to improve the disturbance suppression ability of the electro-optical tracking system. Meanwhile, this article uses RSLQR method to improve the dynamic response performance of the system. Considering the influence of

weighting matrix in the RSLQR method on system's performance, this article presents a selection criterion of weighting matrix in the RSLQR to meet the performance requirements of closed-loop system. Through simulation analysis and experimental verification, the proposed RSLQR method based on LESO has great advantages in dynamic response of the system and disturbance suppression ability of the system. With the increase of target tracking mobility in the electro-optical tracking system, the system has the problem of low tracking accuracy. The next plan is to combine the design method of high-type control loop with the method proposed in this article to enhance and improve the performance of the system.

Declaration of conflicting interests

The author(s) declared no potential conflicts of interest with respect to the research, authorship, and/or publication of this article.

References

[1] Y. Luo, W. Xue, W. He, K. Nie, Y. Mao, and J. M. Guerrero, "Delay-compound-Compensation control for photoelectric tracking system based on improved smith predictor scheme," *IEEE Photon. J.*, vol. 14, no. 3, Jun. 2022, Art. no. 6625708.

[2] C. Tu, J. Shen, J. Dai, L. Zhang, and J. Wang, "A lower size, weight acquisition and tracking system for airborne quantum communication," *IEEE Photon. J.*, vol. 14, no. 6, Dec. 2022, Art. no. 7356908.

[3] Q. Duan et al., "Add-on integration module-based proportional-integration-derivative control for higher precision electro-optical tracking system," *Trans. Inst. Meas. Control*, vol. 43, no. 6, pp. 1347–1362, 2021.

[4] W. Ren et al., "Stabilization control of electro-optical tracking system with fiber-optic gyroscope based on modified smith predictor control scheme," *IEEE Sensors J.*, vol. 18, no. 19, pp. 8172–8178, Oct. 2018.

[5] K. Nie et al., "Disturbance observer-based repetitive control with application to optoelectronic precision positioning system," *J. Franklin Inst.*, vol. 358, no. 16, pp. 8443–8469, 2021.

[6] J. Deng et al., "On dual compensation to disturbances and uncertainties for inertially stabilized platforms," *Int. J. Control, Automat. Syst.*, vol. 20, no. 5, pp. 1521–1534, 2022.

[7] Y. Luo et al., "Multiple fusion based on the CCD and MEMS accelerometer for the low-cost multi-loop optoelectronic system control," *Sensors*, vol. 18, no. 7, 2018, Art. no. 2153.

[8] C. Deng, Y. Mao, and G. Ren, "MEMS inertial sensors-based multi-loop control enhanced by disturbance observation and compensation for fast steering mirror system," *Sensors*, vol. 16, no. 11, 2016, Art. no. 1920.

[9] Y. Mao et al., "Characteristic analysis and robust control design of double-stage precision stabilized platform," *Sensors Actuators A: Phys.*, vol. 300, 2019, Art. no. 111636.

[10] C. Deng, T. Tang, Y. Mao, and G. Ren, "Enhanced disturbance observer based on acceleration measurement for fast steering mirror systems," *IEEE Photon. J.*, vol. 9, no. 3, 2017, Art. no. 6802211.

[11] Q. Dong, Y. Liu, Y. Zhang, S. Gao, and T. Chen, "Improved ADRC with ILC control of a CCD-based tracking loop for fast steering mirror system," *IEEE Photon. J.*, vol. 10, no. 4, 2018, Art. no. 6601314.

[12] Y. Ma et al., "MPPT control of photovoltaic system combined with correction link and LADRC," in *Proc. IEEE Int. Conf. Mechatron. Automat.*, 2021, pp. 426–430.

[13] W. Wei, Z. Zhang, and M. Zuo, "Phase leading active disturbance rejection control for a nanopositioning stage," *ISA Trans.*, vol. 116, pp. 218–231, 2021.

[14] K. Łakomy and R. Madonski, "Cascade extended state observer for active disturbance rejection control applications under measurement noise," *ISA Trans.*, vol. 109, pp. 1–10, 2021.

[15] Z. Wu et al., "On transitioning from PID to ADRC in thermal power plants," *Control Theory Technol.*, vol. 19, pp. 3–18, 2021.

[16] L. Liu, M. Chen, and T. Li, "Disturbance observer-based LQR tracking control for unmanned autonomous helicopter slung-load system," *Int. J. Control, Automat. Syst.*, vol. 20, no. 4, pp. 1166–1178, 2022.

[17] A. Alalwan et al., "Extended kalman filter based linear quadratic regulator control for optical wireless communication alignment," *IEEE Photon. J.*, vol. 12, no. 6, Dec. 2020, Art. no. 7907012.

[18] X. Yu et al., "Atmospheric turbulence suppression algorithm based on APD adaptive gain control for FSO links of 5 G floating base stations," *IEEE Photon. J.*, vol. 12, no. 4, Aug. 2020, Art. no. 7904011.

[19] R. Liu et al., "Machine learning based visible light indoor positioning with single-LED and single rotatable photo detector," *IEEE Photon. J.*, vol. 14, no. 3, Jun. 2022, Art. no. 7322511.

[20] L. Fan et al., "Design of LQR tracking controller combined with orthogonal collocation state planning for process optimal control," *IEEE Access*, vol. 8, pp. 223905–223917, 2020.

[21] C. Liu et al., "Extending the LQR to the design of PID type–II and type–III control loops," *IET Control Theory Appl.*, vol. 17, no. 6, pp. 713–743, 2023.

[22] G. Zhang et al., "Longitudinal attitude controller design for aircraft landing with disturbance using ADRC/LQR," in *Proc. IEEE Int. Conf. Automat. Sci. Eng.*, 2013, pp. 330–335.

[23] Z. Chen and H. Jia, "Design of flight control system for a novel tilt-rotor UAV," *Complexity*, vol. 2020, pp. 1–14, 2020.

[24] Y. Zhang, J. Jin, and L. Huang, "Model-free predictive current control of PMSM drives based on extended state observer using ultralocal model," *IEEE Trans. Ind. Electron.*, vol. 68, no. 2, pp. 993–1003, Feb. 2021.

[25] Y. Zhang et al., "Robust predictive current control of induction motors based on linear extended state observer," *Chin. J. Elect. Eng.*, vol. 7, no. 1, pp. 94–105, 2021.

[26] Y. Zhang et al., "Extended state kalman filter-based path following control of underactuated autonomous vessels," *Trans. Inst. Meas. Control*, vol. 43, no. 15, pp. 3311–3321, 2021.

[27] Q. Zheng, L. Q. Gao, and Z. Gao, "On validation of extended state observer through analysis and experimentation," *J. Dyn. Syst., Meas. Control*, vol. 134, no. 2, pp. 024505.1–024505.6, 2012.

[28] X. Yang and Y. Huang, "Capabilities of extended state observer for estimating uncertainties," in *Proc. IEEE Amer. Control Conf.*, 2009, pp. 3700–3705.

[29] S Srivastava et al., "An optimal PID controller via LQR for standard second order plus time delay systems," *ISA Trans.*, vol. 60, pp. 244–253, 2016.

[30] C. Liu, Y. Mao, and X. Qiu, "Disturbance-observer-based LQR tracking control for electro-optical system," *Photon. MDPI*, vol. 10, no. 8, 2023, Art. no. 900.

[31] Z. Gao, "Scaling and bandwidth-parameterization based controller tuning," in *Proc. ACC*, 2003, pp. 4989–4996.

[32] C. E. Garcia and M. Morari, "Internal model control. A unifying review and some new results," *Ind. Eng. Chem. Process Des. Develop.*, vol. 21, no. 2, pp. 308–323, 1982.